

PAPER • OPEN ACCESS

Resonant solitary states in complex networks

To cite this article: Jakob Niehues *et al* 2024 *New J. Phys.* **26** 113016






View the [article online](#) for updates and enhancements.

You may also like

- [Steering internal and outgoing electron dynamics in bilayer graphene cavities by cavity design](#)
Lukas Seemann, Angelika Knothe and Martina Hentschel
- [Theory of wetting dynamics with surface binding](#)
Xueping Zhao, Susanne Liese, Alf Honigmann *et al.*
- [Highly scalable quantum router with frequency-independent scattering spectra](#)
Yue Cai, Kang-Jie Ma, Jie Liu *et al.*



PAPER

Resonant solitary states in complex networksJakob Niehues^{1,2,3,*} , Serhiy Yanchuk^{1,4} , Rico Berner² , Jürgen Kurths^{1,2} , Frank Hellmann¹ 
and Mehrnaz Anvari^{1,5}¹ Potsdam Institute for Climate Impact Research (PIK), Member of the Leibniz Association, PO Box 60 12 03, D-14412 Potsdam, Germany² Department of Physics, Humboldt-Universität zu Berlin, Newtonstraße 15, 12489 Berlin, Germany³ Technische Universität Berlin, ER 3-2, Hardenbergstrasse 36a, 10623 Berlin, Germany⁴ School of Mathematical Sciences, University College Cork, Western Road, Cork T12 XF62, Ireland⁵ Fraunhofer Institute for Algorithms and Scientific Computing, 53757 Sankt Augustin, Germany

* Author to whom any correspondence should be addressed.

E-mail: jakob.niehues@pik-potsdam.de**Keywords:** coupled oscillator networks, network stability, network topology, power grids, second-order Kuramoto model, solitary statesSupplementary material for this article is available [online](#)

OPEN ACCESS

RECEIVED
12 July 2024REVISED
17 October 2024ACCEPTED FOR PUBLICATION
25 October 2024PUBLISHED
21 November 2024Original Content from
this work may be used
under the terms of the
[Creative Commons
Attribution 4.0 licence](#).Any further distribution
of this work must
maintain attribution to
the author(s) and the title
of the work, journal
citation and DOI.**Abstract**

Partially synchronized solitary states occur frequently when a synchronized system of networked oscillators with inertia is perturbed locally. Several asymptotic states of different frequencies can coexist at the same node. Here, we reveal the mechanism behind this multistability: additional solitary frequencies arise from the coupling between network modes and the solitary oscillator's frequency, leading to significant energy transfer. This can cause the solitary node's frequency to resonate with a Laplacian eigenvalue. We analyze which network structures enable this resonance and explain longstanding numerical observations. Another solitary state that is known in the literature is characterized by the effective decoupling of the synchronized network and the solitary node at the natural frequency. Our framework unifies the description of solitary states near and far from resonance, allowing to predict the behavior of complex networks from their topology.

1. Introduction

Many natural and human-made systems are characterized by various degrees of synchronization, which is one of the most fundamental common aspects of their collective behavior [1]. Therefore, important extended systems as diverse as the heart, the brain, firefly populations, chemical reactions, and power grids, are ubiquitously modeled as networks of interconnected oscillators [2–6]. In some, such as power grids, global synchronization is essential for their proper functioning, in others, such as the brain, it can indicate severe dysfunction. The tendency to synchronize, and thus the function of the system, is strongly influenced by the underlying network's topology.

The paradigmatic models for understanding this relationship between structure and function in coupled oscillator networks are the Kuramoto model [7] and its variants. These models feature extremely rich collective behavior, such as chimera states, frequency clusters, isolated desynchronization, and spatial chaos [2–9]. The Kuramoto model with inertia [10, 11] has been developed independently to study synchronization properties in power grids [12, 13] and biological systems [14].

The transition from decoupling to synchrony in Kuramoto networks is characterized by spatial chaos, a form of extreme multistability [15]. This regime typically has several states with similarly sized basins of attraction [16, 17]. Among the most prominent are frequency clusters [18, 19], the simplest of which are solitary states. In a solitary state, only one or a few independent oscillators are phase-shifted [20] or, in the presence of inertia, start to rotate at their own frequencies [21], while the rest of the network remains synchronized. Solitary states are especially prominent for the important situation of localized large perturbations [22–24] and they are particularly likely for perturbations at leaf nodes [22, 25]. Localized perturbations are important in systems like power grids, where single component failures are common and can lead to desynchronization and blackouts [26].

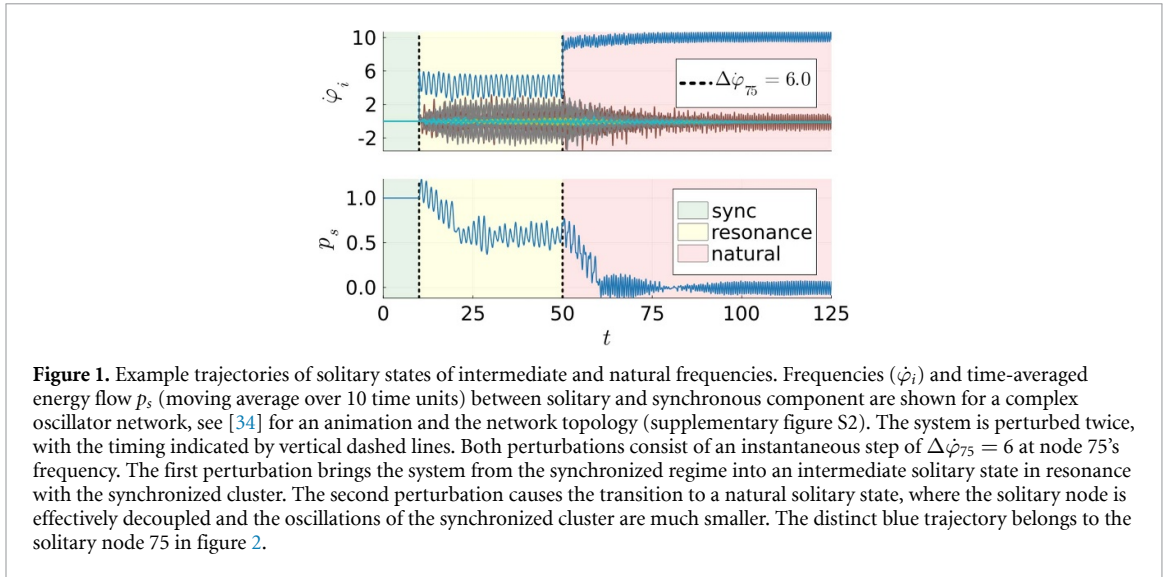


Figure 1. Example trajectories of solitary states of intermediate and natural frequencies. Frequencies (φ_i) and time-averaged energy flow p_s (moving average over 10 time units) between solitary and synchronous component are shown for a complex oscillator network, see [34] for an animation and the network topology (supplementary figure S2). The system is perturbed twice, with the timing indicated by vertical dashed lines. Both perturbations consist of an instantaneous step of $\Delta\varphi_{75} = 6$ at node 75's frequency. The first perturbation brings the system from the synchronized regime into an intermediate solitary state in resonance with the synchronized cluster. The second perturbation causes the transition to a natural solitary state, where the solitary node is effectively decoupled and the oscillations of the synchronized cluster are much smaller. The distinct blue trajectory belongs to the solitary node 75 in figure 2.

Interestingly, numerical studies have revealed that solitary nodes can exist not only at the natural frequency of the oscillators, but also at intermediate frequencies [17, 25]. In addition, the presence of multistability in these solitary nodes has been identified, allowing for the coexistence of both intermediate and natural solitary states [17, 25] at the same node.

Previous work has discussed the role of a networks' topology in understanding its overall response to perturbations and the emergence of various stable states [6, 22, 25, 27, 28]. In some contexts, the frequency and stability of the solitary states have been studied in terms of decoupling and entrainment arguments [23, 29]. These explanations do not account for either intermediate frequency solitaries or the coexistence of several solitary states at the same node.

In this work, we use averaging theory [30] and linear response to develop a theory of the resonant coupling between the synchronized cluster and the solitary node. We uncover that the described phenomena arise from the cluster's resonantly excited complex network structure. This leads to a non-zero mean energy flow between the synchronized cluster and the solitary node, and a frequency shift (figure 1). While works like [31–33] have previously considered the interaction between individual oscillators and the mean field, such an interaction between collective network modes and individual oscillators has not been previously described. Here, we uncover how the network's topology shapes the landscape of solitary states and illustrate our findings with a range of example systems, ranging from conceptual models to fully complex networks.

2. Model

In the following, we will use the Kuramoto model with inertia on complex networks [10, 11, 22, 23, 28, 35, 36]. It is given by the coupled second-order equations

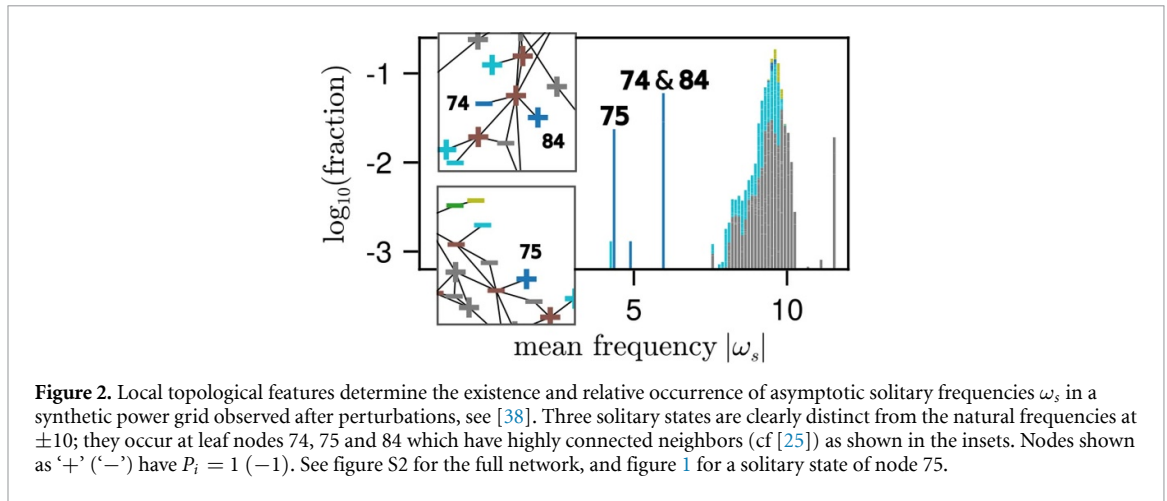
$$m_i \ddot{\varphi}_i = P_i - \alpha_i \dot{\varphi}_i - \sum_{j=1}^N p_{ij}(\varphi_i, \varphi_j), \quad (1)$$

where φ_i are the phases of the N oscillators, P_i the driving powers, the m_i are inertia constants, and the $\alpha_i > 0$ are damping coefficients. The coupling is given in terms of the weighted coupling matrix $\{\kappa_{ij}\}$ as

$$p_{ij}(\varphi_i, \varphi_j) = \kappa_{ij} \sin(\varphi_i - \varphi_j). \quad (2)$$

Note that the coupling matrix is symmetric, $\kappa_{ij} = \kappa_{ji}$, hence the coupling function is antisymmetric, $p_{ij} = -p_{ji}$. We parametrize the model equation (1) such that the synchronous state coexists with various stable attractors of different degree of synchronization. In particular, we set $P_i = 1$ for producers, $P_i = -1$ for consumers, $\alpha_i = 0.1$, and $\kappa_{ij} = 6$ for connected nodes (i, j) . This is the parameter regime of, for example, real-world power grids [17, 22, 23, 25, 35].

To better understand the asymptotic behavior of the system, we recall a few properties of its attractors. In a synchronous state, we have $\varphi_i(t) = \varphi_i^* + \hat{\omega}t$, and constant frequencies $\dot{\varphi}_i^* = \hat{\omega}$, and the phases satisfy $P_i - \alpha_i \hat{\omega} = \sum_{j=1}^N p_{ij}(\varphi_i^*, \varphi_j^*)$. By going to a corotating frame via $\varphi_i \rightarrow \varphi_i - \hat{\omega}t$, we can always set $\hat{\omega} = 0$, and will assume so from now on. The $p_{ij}(\varphi_i^*, \varphi_j^*)$ can be interpreted as the energy flowing through the network to



balance out the driving powers P_i , (this is the physical interpretation for power grids), and α_i determines the restoring force of the frequency. The natural frequencies of the uncoupled oscillators (i.e. when all $\kappa_{ij} = 0$) are determined by the condition that driving power and restoring force are in balance: $\Omega_i := P_i/\alpha_i$. Solitary states in systems of coupled oscillators can be quite similar to the natural solitary states of uncoupled oscillators, which can serve as an approximation [22].

In this work we consider so-called *frequency solitary states*, in which one or a few independent oscillators rotate at a distinct frequency, while the rest of the network forms a large synchronized cluster. For simplicity, we restrict ourselves to 1-solitarys, which have only a single solitary oscillator at a node that we denote z . However, the considerations in this work apply to the case of several solitary nodes as well, see supplemental material [34], section I.F (SM I.F). We denote the synchronized cluster $S = \{i : 1 \leq i \leq N, i \neq z\}$, and the long-term time average by $\langle \cdot \rangle$. Then, for the purpose of this work, a solitary state is defined by $\langle \dot{\varphi}_z(t) \rangle = \omega_s$ and $\langle \varphi_i(t) \rangle = \omega_{\text{sync}}$, with $\omega_s \neq \omega_{\text{sync}}$. Such solitary states only exist in the presence of inertia [24].

To illustrate the phenomenon we describe and explain in this paper, we show simulation results in figure 2. It displays the different asymptotic frequencies actually observed following single node perturbations in a complex network, the topology of which was generated with [37]. The $|\omega_s|$, that coincide with $\omega_s \cdot \text{sgn}(P_z)$, are the absolute values of the mean asymptotic solitary frequencies ω_s of the trajectories $\dot{\varphi}_z(t)$ at the solitary nodes z . The trajectories are won from integrating equation (1) from many initial conditions generated by perturbing the synchronous state (see [38] for code and details). Here, asymptotic states are counted as 1-solitary if there is exactly one node with frequency $|\omega_s| > 1$, cf figure S4. Note that many solitary frequencies are close to the natural frequencies at $\Omega_i = \pm 10$. We define such solitary states with $\omega_s \approx \Omega_z$ as *natural*. However, when perturbations occur at nodes 74, 75 and 84, they can also induce intermediate frequencies. We define solitary states with such intermediate mean frequency $|\omega_s| < |\Omega_z|$ as *resonant*, because (i) the fluctuation of the nodes in S is more excited (see figure 1), and (ii) because we show that ω_s is in resonance with a network mode. The nodes 74, 75 and 84 share a specific topological property: they are leaf nodes (degree-1 nodes) with a high-degree neighbor. The intermediate resonant solitary states occur at all such nodes in this network (and other networks), and only at these nodes, discarding marginal effects. We explore this strong link between the topology and the asymptotic behavior of the nodes in the following sections.

3. Ansatz and self-consistency

Here, we present our main result: the framework that allows us to make predictions of solitary states and relate them to the network’s topology. The framework predicts the existence and stability of both natural and resonant solitary states. It consists of an ansatz and a self-consistent equation it has to fulfill.

An ansatz is a proposed form of a solution, often justified by prior knowledge about the system, and its sole purpose is to insert it and evaluate the result it produces. Here, the ansatz is a change of coordinates without loss of generality.

We begin by introducing suitable notation for describing a solitary leaf node z and a synchronized cluster $S = \{i : 1 \leq i \leq N, i \neq z\}$. For simplicity, we will assume that α_i and m_i are constant throughout S . Node z is connected to S through the intermediary node $k \in S$. With all introduced notations, the considered system has the form

$$m\ddot{\varphi}_i = P_i - \alpha\dot{\varphi}_i - \sum_{j=1}^N \kappa_{ij} \sin(\varphi_i - \varphi_j), \quad i \in S, \quad (3)$$

$$m_z\ddot{\varphi}_z = P_z - \alpha_z\dot{\varphi}_z - \kappa_{zk} \sin(\varphi_z - \varphi_k). \quad (4)$$

The coupling between subsystems S and z is given by p_{zk} , which we decompose into a long-term time average $p_s := \langle p_{zk} \rangle$ and a mean zero part $p_{zk}^{\text{osc}}(t)$:

$$p_{zk}(t) = \kappa_{zk} \sin[\varphi_z(t) - \varphi_k(t)] := p_s + p_{zk}^{\text{osc}}(t). \quad (5)$$

Note that we do not have an explicit expression for p_s and $p_{zk}^{\text{osc}}(t)$ yet, but obtain them later.

Our ansatz for the trajectories, is to split the linear motion in time with the mean frequency from the mean zero part, similarly to p_{zk} in equation (5),

$$\varphi_i(t) := \omega_{\text{sync}}t + \vartheta_i^* + \vartheta_i(t) \quad \text{for } i \in S, \quad (6)$$

$$\varphi_z(t) := \omega_{\text{sync}}t + \vartheta_k^* + \vartheta_z(t) := \omega_s t + \vartheta_k^* + \varepsilon\psi_z(t), \quad (7)$$

for some small ε that we determine later. We define ω_{sync} and ω_s as the long term average frequency of the synchronized cluster, and the solitary oscillator, respectively. This means $\langle \vartheta_i(t) \rangle = 0 = \langle \psi_z(t) \rangle$ by construction. The ϑ_i^* are a synchronous state of S given a fixed power injection p_s at node k . Note that the ansatz is without loss of generality, and can be formally considered as a change of variables. We use the form equations (6) and (7) because if a solitary state occurs, $\psi_z(t)$ and $\vartheta_i(t)$ are bounded, and the corotating solitary frequency, defined as $\omega_c := \omega_s - \omega_{\text{sync}}$, is non-zero, cf supplementary video 1 [34]. We can use the ansatz equations (5)–(7) to determine the mean-zero part of the solitary trajectory $\psi_z(t)$, however, it is more informative to determine ω_s and p_s from the ansatz as a characterization of the solitary state.

To determine ω_s , we note that a condition for the existence of a solitary state at ω_s is that both ω_s and p_s have to fulfill a self-consistent equation. The argument goes as follows. For $\psi_z(t)$ to stay bounded, and for ω_s to be the long-term average of the solitary node's frequency, the long-term average of $\dot{\vartheta}_z = \varepsilon\dot{\psi}_z$ has to be zero. Demanding this for equation (4) provides us with the condition $0 = P_z - \alpha_z\omega_s - p_s$. We can interpret p_s as a measure for the mean coupling of S and z , while ω_s stands for their incoherence. Note that this relationship between ω_s and p_s can be observed in figure 1: in synchrony ($\omega_s = 0$) there is a steady high energy flow $p_s = P_z$; in the natural solitary state, the mean energy flow $p_s \approx 0$ and the system is effectively decoupled. For intermediate resonant solitary states, there is some intermediate amount of energy transfer $0 < |p_s| < |P_z|$.

If we now can express p_s as a function of ω_s , the above condition for a solitary state to have well-defined frequency becomes a self-consistent equation for ω_s :

$$0 = Z(\omega_s) := P_z - \alpha_z\omega_s - p_s(\omega_s). \quad (8)$$

The self-consistency function $Z(\omega_s)$ is defined as the average change of the solitary frequency as a function of the solitary mean frequency: $Z(\omega_s) := \langle m_z\dot{\vartheta}_z \rangle(\omega_s)$. A potentially stable solitary state at ω_s requires the correct sign of the change in Z with frequency: if a change in ω_s leads to a larger change in ω_s in the same direction, the solitary frequency is linearly unstable, and vice versa. If we imagine ω_s as slowly varying, we have $m_z\dot{\omega}_s = Z(\omega_s)$. Thus, we expect the sign of the derivative $\partial_{\omega_s} Z(\omega_s)$ to be informative about the stability of the solitary state, at least as a proxy. In other words, by introducing the explicitly time-dependent ansatz equations (6) and (7), we get a non-autonomous system from equations (3) and (4). We are looking for limit cycles of this system that correspond to fixed points in the long-term averaged dynamics. These fixed points are solutions ω_s of equation (8): mean frequencies that are allowed to persist by the dynamics, and that are stable under small perturbations.

To obtain the solutions, our strategy is as follows. We assume that we can linearize equations (3) and (4) in $\vartheta_i(t)$ and ε to obtain a system that quantitatively reflects the behavior of the trajectory of the solitary state. We will analyze the linearized system using averaging, and see that this is justified in many regimes. Together with the self-consistent equation, we obtain a proxy system for the description of solitary states. If the proxy system is stable, we conclude that a solitary state can (but is not guaranteed to) exist at ω_s . If the proxy system does not admit a stable solution for specific parameters, we interpret this as evidence that a solitary state cannot exist with those parameters. Numerically, we see that if the proxy system admits a stable solution, we often do find solitary states with a large basin. We interpret this to mean that the mechanism revealed by the proxy system is indeed responsible for the formation and stabilization of solitary states.

To follow the strategy outlined above and evaluate equation (8) to get predictions for solitary frequencies and their stability, we first need to determine p_s as a function of ω_s . We present a derivation in the next section, and an interpretation and alternative derivation thereafter.

4. Averaging

Here, we outline the derivation of our main result, an explicit form for $p_s(\omega_s)$. For a detailed step-by-step instruction, we refer to the supplemental material [34], section I (SM I).

Both p_s and ω_s depend on the trajectories $\varphi_z(t)$ and $\varphi_k(t)$ of the solution to equations (3) and (4). To obtain an explicit approximation of the solution, we will leverage a version of the averaging theorem [30] (and references therein).

We start by giving a brief summary of the averaging method following [30]. Let $0 \leq \varepsilon \ll 1$, and $x \in U \subseteq \mathbb{R}^n$ for a bounded set U . Let $f: \mathbb{R}^n \times \mathbb{R} \times \mathbb{R}^+ \rightarrow \mathbb{R}^n$ be a C^r function with $r \geq 2$ (at least twice continuously differentiable) that is time-periodic with period $T > 0$, and that determines the non-autonomous periodic dynamical system

$$\dot{x} = \varepsilon f(x, t, \varepsilon). \tag{9}$$

Define the associated autonomous averaged system as

$$\dot{y} = \varepsilon \frac{1}{T} \int_0^T f(y, t, 0) dt := \varepsilon \bar{f}(y). \tag{10}$$

The averaging theorem states that a system of the form equation (9) can be cast into the form

$$\dot{y} = \varepsilon \bar{f}(y) + \varepsilon^2 f_1(y, t, \varepsilon), \tag{11}$$

where f_1 is also of period T in t . This can be achieved by a coordinate change. Moreover, solutions $x(t)$ of equation (9) and $y(t)$ of equation (10) that are ε -close stay ε -close on a timescale $t \sim \varepsilon^{-1}$. Further, hyperbolic fixed points of equation (10) have corresponding unique ε -close hyperbolic periodic orbits of the same stability type. We will leverage this theorem as follows: By using the ansatz equations (6) and (7) and appropriate approximations, we cast the system equations (3) and (4) into the form equation (9). In the proper coordinate frame, the system is time-periodic and slowly varying. We can then find approximate solutions by solving its corresponding averaged system for fixed points. Those solutions, in particular $\vartheta_k(t)$, enable us to calculate p_s as a function of ω_s and close the self-consistent equation, equation (8).

First, we need to approximate the highly nonlinear dynamics in equations (3) and (4) appropriately. Since the synchronized oscillators from the cluster S are weakly perturbed by the solitary rotation, we assume smallness of $\vartheta_i(t)$, which is also justified by numerical observations, see figure 1 and [34, 38]. Therefore, we linearize the system equations (3) and (4) with respect to $\vartheta_i(t) \in S$ around the origin. It is crucial not to linearize with respect to $\vartheta_z(t)$, because it is not bounded. For example, the coupling function p_{zk} in equations (4) and (5) is approximated to linear order in ϑ_k as

$$p_{zk}(t) \approx \kappa_{zk} \{ \sin[\omega_c t + \varepsilon \psi_z(t)] - \vartheta_k(t) \cos[\omega_c t + \varepsilon \psi_z(t)] \}. \tag{12}$$

From now on, p_s and $p_{zk}^{\text{osc}}(t)$ represent the mean and oscillating part of the approximated p_{zk} . To write the obtained system in vector form, we define the vectors $e_i^k := \delta_{ik}$, where $\delta_{ik} = 1$ if $i = k$, and $\delta_{ik} = 0$ else.

Introducing $\vec{\vartheta}(t)$ with components $\vartheta_i(t)$ for all $i \in S$, the linearized system is

$$m \ddot{\vec{\vartheta}} = -\alpha \dot{\vec{\vartheta}} - L^* \vec{\vartheta} + e^k p_{zk}^{\text{osc}}(t), \tag{13}$$

$$m_z \ddot{\vartheta}_z = P_z - \alpha_z \left(\dot{\vartheta}_z + \omega_{\text{sync}} \right) - p_s - p_{zk}^{\text{osc}}(t), \tag{14}$$

where L^* is the effective coupling Laplacian on the synchronized cluster with weights $L_{ij}^* = \kappa_{ij} \cos(\vartheta_i^* - \vartheta_j^*)$ and eigenvectors $\vec{v}^{[\ell]}$. We have successfully transformed into a frame that accounts for the power imbalance due to p_s . This can be seen from the fact that p_s does not appear in the equation for S , equation (13), since the synchronized cluster steady state accounts for the average power injection p_s from the solitary node with the ω_{sync} rotation.

Second, we need to properly take care of the fact that equations (13) and (14) become a non-autonomous system when we insert the explicitly time-dependent ansatz equations (6) and (7) into p_{zk} . We introduce a timescale ε^{-1} that splits the autonomous and non-autonomous parts in equations (13) and (14). It allows us to write the system in a perturbative form, in which averaging can be applied. Such a scaling can be achieved, if node k has a sufficiently high degree (SM I.A). In that case, there is a Laplacian eigenvalue $\lambda^{[r]}$ that is highly correlated to the node's degree d_k . We will observe in the examples below that the solitary frequency tunes itself towards resonance with such eigenmodes: $\omega_s^2 \sim \lambda^{[r]}$.

The rescaling is given by

$$t = \sqrt{\frac{m}{\lambda^{[r]}}} t', \quad P_i = \frac{P'_i \alpha \sqrt{\lambda^{[r]}}}{\sqrt{m}}, \quad \kappa_{ij} = \frac{\kappa'_{ij} \alpha \sqrt{\lambda^{[r]}}}{\sqrt{m}}, \quad (15)$$

dropping the prime from now on. Further, we set $\varepsilon = \alpha/\sqrt{m\lambda^{[r]}} \ll 1$. In other words, by rescaling the time axis we can absorb m in equation (13), and set α , P , and κ to ε , εP and $\varepsilon \kappa$. We choose ε such that, while the rescaled κ remains of order one, the eigenvalues of the rescaled effective Laplacian L^* for the eigenmodes localized at k are of order ε^{-1} . As a result, we treat $L^r = \varepsilon L^*$ as being of order one. Equations (13) and (14) become

$$\ddot{\vec{\vartheta}} = \varepsilon \left[-\dot{\vec{\vartheta}} + e^k p_{zk}^{\text{osc}}(t) \right] - L^r \vec{\vartheta}, \quad (16)$$

$$\ddot{\vartheta}_z = \frac{\varepsilon m}{m_z} \left[P_z - \frac{\alpha_z}{\alpha} \dot{\vartheta}_z - p_{zk}(t) \right]. \quad (17)$$

Third, a crucial step for solvability is to approximate $\varepsilon p_{zk}(t)$, cf equation (12), to first order in ε , which finally allows us to identify an explicit expression for p_s in terms of ϑ_k and ω_c ,

$$\varepsilon p_{zk}(t) \approx \varepsilon \kappa_{zk} (\sin \omega_c t - \vartheta_k(t) \cos \omega_c t), \quad (18)$$

$$p_s \approx \kappa_{zk} \langle \vartheta_k(t) \sin \omega_c t \rangle. \quad (19)$$

Equation (16) has the form of the perturbation of the Hamiltonian system $\ddot{\vec{\vartheta}} = -L^r \vec{\vartheta}$, where the perturbation is of order ε . The perturbation is caused partly by the presence of $\vartheta_k(t)$, and by other small terms, such as damping. The appropriate perturbative approach in this case is averaging [30], where one should first write the system for the slowly varying amplitudes $\vec{x}(t)$ and $\vec{z}(t)$ of the network modes $\vec{\xi}(t)$, i.e. the amplitudes of the periodic solutions of the unperturbed system. This is achieved by diagonalization of the Laplacian with the linear transformation $Q_{ij} := v_i^{[j]}$,

$$\vec{\xi}(t) := Q^T \vec{\vartheta}(t) := \vec{x}(t) \cos \omega_c t - \vec{z}(t) \sin \omega_c t. \quad (20)$$

The amplitude dynamics for $\vec{x}(t)$ and $\vec{z}(t)$ can be inferred with the invertible van der Pol transformation (spelled out in equation (S50)) into the frame rotating at the driving frequency ω_c . These amplitude dynamics is then decomposed into modes resonant with ω_c and non-resonant modes. For the sake of brevity and clarity, we refer to SM I for details. Most importantly, the contributions of both types of modes are small for different reasons. On one hand, the resonant modes give small contributions due to a small prefactor $\varepsilon \Delta \sim \omega_c^2 - \lambda^{[r]}$. On the other hand, the non-resonant modes, where $\varepsilon \Delta$ is of $O(1)$, give small contributions due to their weak localization, allowing us to average the dynamics of the slowly varying $\vec{x}(t)$ and $\vec{z}(t)$. We obtain an autonomous system that is a good approximation (ε -close) of the non-autonomous system for time scales up to ε^{-1} [30]. This averaged system (equation (S55)) is linear with a unique solution that gives us the average amplitudes \vec{x}^* and \vec{z}^* of all modes. From those, we obtain the average trajectory of $\vartheta_k(t)$, and insert it into equation (19) to get an expression for $p_s(\omega_s)$. This finally provides us with the explicit form of the self-consistent equation (8):

$$\begin{aligned} 0 = Z(\omega_s) &= P_z - \alpha_z \omega_s - p_s \\ &= P_z - \alpha_z \omega_s - \frac{\kappa_{zk}^2}{2} \sum_{\ell=1}^{N-1} \frac{\alpha \omega_c \left(v_k^{[\ell]} \right)^2}{\left(\lambda^{[\ell]} - m \omega_c^2 \right)^2 + \alpha^2 \omega_c^2}. \end{aligned} \quad (21)$$

In equation (21), the sum runs over eigenmodes ℓ of L^* , with eigenvalue $\lambda^{[\ell]}$ and eigenvector $\vec{v}^{[\ell]}$. To efficiently evaluate equation (21), we assume that the dependence of L^* and its eigenmodes on p_s is weak. This is a reasonable assumption if the synchronized cluster is significantly larger than the solitary cluster (node z), and the energy injected at node k dissipates quickly into S . Practically, the ϑ_i^* , that depend on p_s , can be well approximated by the φ_i^* , that do not (SM I.B).

Lastly, to close equation (21), we need to relate the solitary frequency ω_s to ω_c , its relative value to S . It can be shown by summing over equation (1) for all $i \in S$ and $i = z$, that the α -weighted sum of frequencies decays towards zero from all initial conditions, hence $(N-1)\alpha\omega_{\text{sync}} + \alpha_z\omega_s = 0$ (see SM I.A.). This gives us

$$\omega_c(\omega_s) = \left(1 + \frac{\alpha_z}{(N-1)\alpha} \right) \omega_s. \quad (22)$$

This linear relationship between ω_s and ω_c is useful in solving equation (21).

Having obtained an explicit, closed, self-consistent equation for ω_s from our ansatz, we now turn to its interpretation and evaluation to make predictions of solitary attractor states and compare them to simulations.

5. Interpretation: a linear response picture

In this section, we provide an alternative derivation that is a shortcut to equation (21), using linear response theory. For an extensive account of linear response in inertial Kuramoto networks, we refer to [28]. As a motivation, we start by discussing the natural interpretation that the linear response offers, and that can also be deduced from the resulting equation (21).

The obtained form of p_s in equation (21) has a natural interpretation. The solitary state, with frequency ω_s , perturbs the synchronized cluster S , with relative frequency ω_c . The response $\vartheta(t)$ of the cluster S oscillates at frequency ω_c with amplitudes a_i and some well-defined phase shifts δ_i , e.g. $\vartheta_k(t) \sim a_k \sin(\omega_c t + \delta_k)$. The phase shift δ_k enables a non-zero energy flow p_s between S and z , which is responsible for maintaining the relative frequency shift ω_c . The energy flow is proportional to the amplitude of the response, and especially the local amplitude of the corresponding eigenvector $v_k^{[\ell]}$ for each mode ℓ . Thus, large energy flows can occur if ω_c is close to resonance with an eigenmode of S that is localized at k . As ω_c determines the magnitude of energy flow, but also shifts with the energy flow itself, the system can robustly tune itself towards such resonances if they are present. This resonant tuning mechanism predicts why certain topological features, namely the ones causing highly localized modes, enable the generation of additional solitary states, cf section 6.

Following this interpretation, we can directly derive the result for $Z(\omega_s)$ in equation (21) using linear response theory, see SM I.C. We observe that the nonlinear part of $p_{zk}^{\text{osc}}(t)$ in equation (16) is eventually averaged out in the averaging approach. Linear response can be readily applied, if we neglect this nonlinearity from the outset. The assumption that this nonlinearity is sufficiently small can be justified, when it is only one of several contributions to the overall coupling of a well-connected node k . In this case, the cluster S is harmonically driven by $\sin \omega_c t$, and linear response similar to [28] can be used to calculate its response for each network mode ℓ separately, including the modal amplitudes $a_i^{(k)[\ell]}(\omega_c)$ at node i and modal phase lags $\delta^{[\ell]}(\omega_c)$ given by

$$a_i^{(k)[\ell]}(\omega_c) := \frac{\kappa_{kz} v_i^{[\ell]} v_k^{[\ell]}}{\sqrt{(\lambda^{[\ell]} - m\omega_c^2)^2 + \alpha^2 \omega_c^2}}, \quad (23)$$

$$\sin \delta^{[\ell]}(\omega_c) := -\frac{\alpha \omega_c}{\sqrt{(\lambda^{[\ell]} - m\omega_c^2)^2 + \alpha^2 \omega_c^2}}. \quad (24)$$

Here, the superscript (k) indicates that the perturbation caused by φ_z enters S at node k . For each mode ℓ , the nodal amplitudes depend on the mismatch between the driving frequency ω_c and the eigenmodes of the network associated with the $\lambda^{[\ell]}$, as well as the localization of the corresponding eigenvectors at nodes i and k . The damping slightly shifts the location of the resonance peaks in the amplitude away from $\omega_c = \pm \sqrt{\lambda^{[\ell]}/m}$ and makes their height finite.

Combining the modal responses linearly provides us with a trajectory for the ϑ_i ,

$$\kappa_{kz} \vartheta_i^{(k)}(t) = \sum_{\ell=1}^{N-1} a_i^{(k)[\ell]} \sin(\omega_c t + \delta^{[\ell]}). \quad (25)$$

From the trajectory of ϑ_k we can determine the time averaged energy flow $p_s = \langle p_{zk} \rangle$ in terms of the amplitudes and phase lags:

$$p_s(\omega_c) = -\frac{\kappa_{kz}}{2} \sum_{\ell=1}^N a_k^{(k)[\ell]}(\omega_c) \sin \delta^{[\ell]}(\omega_c) \quad (26)$$

$$= \frac{\kappa_{zk}^2}{2} \sum_{\ell=1}^{N-1} \frac{\alpha \omega_c (v_k^{[\ell]})^2}{(\lambda^{[\ell]} - m\omega_c^2)^2 + \alpha^2 \omega_c^2}, \quad (27)$$

which is the exact same as in equation (21). In fact, the terms in the denominators in the sum over all modes in equation (21) resemble the resonance curve of linear oscillators. It is known as Cauchy–Lorentz

distribution, Lorentz(ian) function, or Breit–Wigner distribution. Due to the generalization to the resonance of a network S , the Lorentzians are summed over all $N - 1$ network modes associated to the $\lambda^{[\ell]}$. Each contribution is weighted by the localization of the corresponding eigenvector $\vec{v}^{[\ell]}$ at node k , quantified by $\left(v_k^{[\ell]}\right)^2$. This is how the topology affects the distribution of resonance in the network, see also [28].

We remark that both approaches used to derive equation (21) straightforwardly generalize to a solitary node connected to several nodes in S , see SM I.D. The back-reactions of the network combine linearly, and we simply sum over all neighbors of z (equation (S74)).

Furthermore, a treatment of heterogeneous system parameters within S is also possible, see SM I.E.

6. Evaluation

Here, we make some general statements about the properties and solutions of our main result, equation (21), and provide some examples.

First, note that the obtained expression for $p_s = \langle p_{zk} \rangle$ in equation (21), has the same sign as ω_c . Therefore, p_s is antisymmetric in ω_c and hence in $\omega_s \sim \omega_c$, cf equation (22). It follows that equation (21) is invariant under $\omega_s \rightarrow -\omega_s$ while $P_z \rightarrow -P_z$, i.e. generators and consumers behave similarly with their solitary frequencies having opposite signs. In fact, it is easy to see from equation (21) that all solutions lie between zero and the natural frequency, $0 \leq |\omega_s| \leq |\Omega_z| = |P_z|/\alpha_z$. We see these bounds and symmetry properties confirmed in figure 2, and the examples below.

As discussed above, the linear stability of solutions of $Z(\omega_s) = 0$ can be heuristically determined by evaluating the derivative: the orbit at ω_s is indicated to be linearly stable if $\partial_{\omega_s} Z(\omega_s) < 0$ and linearly unstable if $\partial_{\omega_s} Z(\omega_s) > 0$. This consideration gains importance with the numerical observation that the instantaneous solitary frequency $\dot{\varphi}_z(t)$ oscillates with time around ω_s , cf figure 1. The solution to $Z(\omega_s) = 0$ is an intersection of $p_s(\omega_s)$ and the straight line $P_z - \alpha_z \omega_s$ with slope $-\alpha_z$. Therefore, stability is given if $-\alpha_z < \partial_{\omega_s} p_s(\omega_s)$. Graphically, this means that $p_s(\omega_s)$ intersects the straight line from below, counting in positive ω_s direction.

The existence of solitary frequencies ω_s as solutions to equation (21) relies on sufficiently high eigenvector localization at the neighboring node k , quantified by $\left(v_k^{[\ell]}\right)^2$. Such high localization is present in random networks of high degree heterogeneity [39]. Indeed, we observe in figure 2 and in the examples below that resonant solitary states are most common at degree-one nodes with a high degree neighbor [25], and that the solitary frequency scales with the degree d_k of node k . For an estimate of the relation between the eigenvector localization, the corresponding eigenvalue and the node's degree, we refer to SM I.A.

The existence of solutions to equation (21) also depends on system parameters and their topological distribution. Whether and which solitary states exist in a complex system is a complex question with no easy answer, but we can provide some insights (see SM II.D for more details). Generally, the parameters need to be chosen in an intermediate regime, such that the synchronous state is not globally attractive, but the coupling is also not too weak. Relatively small damping α_i and strong coupling κ_{ij} , such as in power grids, are an indicator for this. We remark that solving the self-consistent equation (21) is an efficient way to determine which solitary states exist. Numerical simulations of the dynamics as in figure 2 are more precise but more expensive.

We now illustrate the power of equation (21) using two examples. First we give a minimal effective model that exhibits the resonant tuning mechanism cleanly; then a full complex network with a complex resonant response. We compare the results with numerical simulations [40]. Further examples can be found in the SM II.B.

6.1. Example I: Two-node model

A minimal model that still shows tristability with two distinct solitary frequencies is a system that neglects the response of the network beyond the node k . We have a solitary node ($z = 1$), its neighbor ($k = 2$), and the rest of the network is assumed to have infinite inertia, and thus no dynamics. This model is shown in the inset in figure 3(right). The neighbor has n links into the infinitely inert part, each with coupling strength K . See SM II.A for details.

The left panel in figure 3 shows the graphical solution of equation (21) for this example system. We see the energy absorbed in node 1 by frequency adaptation, a straight line given by $P_1 - \alpha \omega_s$, and the energy flow due to the network's response, $p_s(\omega_s) = \langle p_{12} \rangle(\omega_s)$. The energy flow has a single peak centered around the only network mode, which is close to $\lambda \approx Kn$. At the intersections of these two curves, we have zeros of equation (21). However, the linear stability heuristic suggests that only intersections with $\partial_{\omega_s} Z < 0$ are candidates for stable solitary states. Indeed, numerical simulations confirm the existence of the stable solutions, and that they correspond to the intersections, where p_s comes from below.

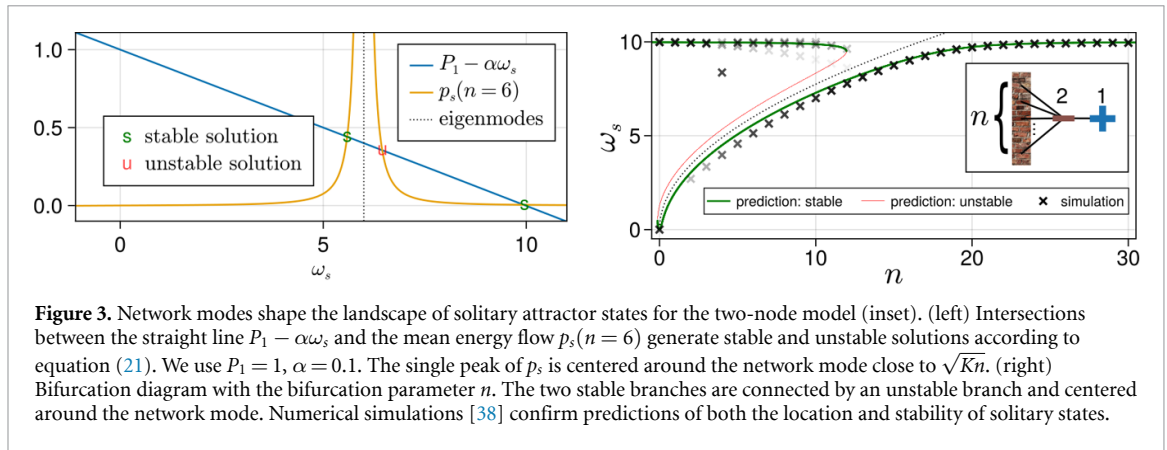


Figure 3. Network modes shape the landscape of solitary attractor states for the two-node model (inset). (left) Intersections between the straight line $P_1 - \alpha\omega_s$ and the mean energy flow $p_s(n = 6)$ generate stable and unstable solutions according to equation (21). We use $P_1 = 1, \alpha = 0.1$. The single peak of p_s is centered around the network mode close to \sqrt{Kn} . (right) Bifurcation diagram with the bifurcation parameter n . The two stable branches are connected by an unstable branch and centered around the network mode. Numerical simulations [38] confirm predictions of both the location and stability of solitary states.

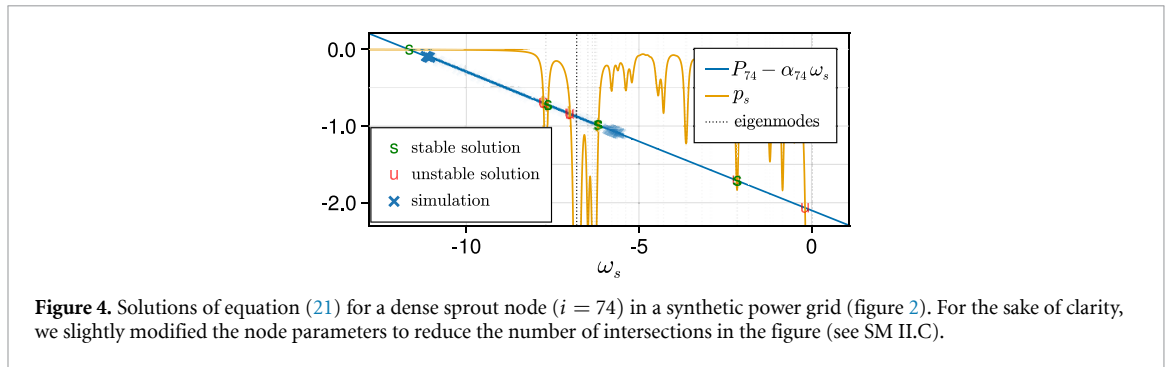


Figure 4. Solutions of equation (21) for a dense sprout node ($i = 74$) in a synthetic power grid (figure 2). For the sake of clarity, we slightly modified the node parameters to reduce the number of intersections in the figure (see SM ILC).

Repeating this solution process for equation (21) for a range of n , we can draw the bifurcation diagram in figure 3(right). Each vertical slice corresponds to the top view of an intersection plot like the one in the left panel. For this minimal example system, we can obtain an explicit expression for several branches $n(\omega_s)$ of stable or unstable solutions (see SM II.A) that correspond to the intersections in the left panel. These branches predict that for $n \lesssim 12$, there is a pair of a stable and an unstable solution ω_s due to the resonance peak around λ , and a third, stable solution at $\omega_s \approx \Omega_1 = P_1/\alpha$. For larger values of n , the second and third solutions annihilate, while the first converges to $\omega_s \rightarrow \Omega_1$. Numerical simulations with random initial conditions [38] closely correspond to the predicted frequency and stability of solitary states, confirming the existence of tristability between the synchronous state and solitary states at multiple frequencies, and confirming the overall accuracy of our results.

In summary, this minimal example system shows that the resonant (intermediate) solitary state and the natural (decoupled) solitary state are two ends of a spectrum of frequencies, and connected by an unstable branch of solutions. Further, the natural frequency is an upper bound for solitary frequencies and can be approached by tuning the resonant network mode higher.

6.2. Example II: Complex network

We now apply our result to the complex network shown in figures 2 and S2. For models of this complexity, the self-consistent equation has to be solved numerically for every node. We observe that intermediate resonant solitary states are located at leaf nodes with neighbor degree ≥ 6 , (cf [25]). Figure 4 shows the solutions of equation (21) for $z = 74$ for slightly heterogeneous parameters.

As many network modes are excited, the response curve $p_s(\omega_s)$ is considerably more complex than for the two-node model. However, simulation results reveal that there is still one dominant mode with high localization at the root node k . Solitary states obtained from random initial conditions are frequently found in close resonance with the dominant mode, or close to the natural frequency.

There are several tentative observations we can make by looking at complex networks, (see also SM II.C, figures S5 and S6 for more examples): (i) If the self-consistent equation yields more solitary states than the one at the natural frequency, there are two dominating solitary states: the one at the natural frequency, and one in resonance with a localized network mode. There can also be many additional solutions with small basins of attraction, cf figures S4 and S5.

(ii) equation (21) tends to overestimate the magnitude of the most prominent solution for ω_s slightly, which can already be observed in the effective model (cf figures 3 and 4). (ii) The most prominent natural

solitary state lies at an intermediate frequency that has a high and broad peak in p_s and some distance to the next solutions. This can be understood by considering that every peak in p_s produces a pair of solutions, a stable one and an unstable one, and that the solitary frequency $\varphi_z(t)$ is modulated around ω_s , cf figure 1. Leaf nodes with high neighbor degree [25], typically produce such situations (cf SM I.A) with a highly localized network mode that results in a high peak. Thus, these findings explain why such nodes feature resonant solitary states with intermediate frequencies. (iii) Besides the main peak at the most localized network mode, there can be several minor peaks that result in solitary states with much smaller basins of attraction due to three reasons: First, the peaks might be narrow, such that the stable and unstable solution are close, second, the peak might not exceed the intersection with the straight line by much, hence the pair of solutions is already close to their annihilation bifurcation, and third, the peak might be close to other peaks and their solutions. This can account for the observation that parts of the phase space can be dominated by basin boundaries of many, different, unlikely states [16], inducing transient chaos [17].

As a closing remark, the derivation of the minimal model, and the explicit relationship between network mode and neighbor degree (SM I.A and II.A), suggest the following. Even in complex networks, the neighbor degree d_k can serve as an upper bound for the (squared) intermediate solitary frequency, when weighted with the coupling κ_{ij} . This is also observed numerically (figure S8).

7. Summary and discussion

We present an analytical description of the effective coupling between a solitary oscillator and the synchronized cluster in a complex network. To approximate the trajectories, we utilize partial linearization and an averaging theorem. This way, we discover that a resonant excitation of the linear modes of the synchronized cluster can couple coherently to the shifted frequency of the solitary state, resulting in a large energy flow between the synchronized cluster and the solitary oscillator, and effectively shifting the frequency.

We have mainly found that intermediate solitary states, first observed in [25], are actually resonant solitary states, and we have uncovered how the network's topology shapes their properties. Furthermore, we have unified their analytical description with the one of natural solitary states [22], and shown that there is a spectrum connecting those extremes.

Our self-consistent framework predicts solitary states in reduced models, where it is solvable, and is also in excellent agreement with what we observe numerically in the original complex networks. With this structure-function relationship, we can explain the observation that solitary states appear mostly in specific parts of the network [18], more specifically leaf nodes and tree-shaped structures, which act as weak points in perturbation scenarios [17, 22, 25, 35]. These results have important implications for improving grid stability through modifications of parameters [41–43] and topology [22, 44–46]: our framework can be used to evaluate how these modifications affect the presence and stability of potentially harmful solitary attractors and their proximity to the synchronous state. Furthermore, we can efficiently identify the troublemaker nodes that tend to desynchronize the easiest due to their intermediate frequencies: resonant solitary states at certain leaf nodes (dense sprout nodes, see [25, 34]). We can identify them from the network topology only, and without expensive simulations. It has been shown that targeted control of such troublemaker nodes can improve grid stability drastically [47].

8. Conclusion and outlook

While the presented mechanism can explain the potential existence and stability of resonant solitary states, there are still open questions that require further investigation. A key practical question is the estimation of the basin boundaries of these states, which would provide deeper insights into the dynamics and robustness of synchronous systems against perturbations [17, 33, 35, 36, 48]. It is known that the basin boundaries depend on the phase and frequency [17, 22, 23]. Averaging the phase dependence out, an estimate of the basin boundaries in ω -direction could be estimated by the turning points of $Z(\omega)$ around a stable solution.

Detailed numerical studies suggest that additional classes of attractive states exist, and the interaction of losses on the lines and resonant energy flow remains unexplored [23]. Furthermore, a more detailed study of the interaction of multiple solitary nodes with distinct frequencies or in frequency clusters is needed (see SM I.F for an outline).

Finally, while this paper focuses on explaining a known phenomenon of Kuramoto oscillators, which exhibit a purely sinusoidal coupling, our derivation generally only demands a 2π -periodic coupling function. This includes coupling functions with phase shifts and harmonics. It would also be interesting to treat phase-amplitude oscillators that play a central role in networks such as power grids [49]. We expect that the overall analytical approach we introduced is a promising tool in describing the synchronization of rotation and oscillation, and leave it to future work to develop and adapt our theory to address a wide range of models.

Data availability statement

The data that support the findings of this study are openly available at the following URL/DOI: [10.5281/zenodo.12636089](https://doi.org/10.5281/zenodo.12636089).

Acknowledgments

Initial investigations of this phenomenon grew out of work by Anton Plietzsch and discussions with Paul Schultz, Chris Bick, Jeroen Lamb, Deniz Eroglu, Tiago Pereira, and Carsten Grabow during a stay at Nesim Mathematics Village.

Part of this work was funded by the DFG Grant CoCoHype (DFG KU 837/39-2; J N, J K, F H, M A) and BMWK Grant OpPoDyn (03EI1071A; J N, F H).

J N gratefully acknowledges support by Studienstiftung des Deutschen Volkes scholarship foundation and Berlin International Graduate School in Model and Simulation based Research (BIMoS) at Technische Universität Berlin. S Y and J K acknowledge funding by DFG, German Research Foundation, Project No. 411803875.

Code availability

The numerical experiments were conducted with the `PowerDynamics.jl` package [40]. Further details can be found in SM III. The code for reproducing our simulations and figures can be found in [38]. The repository can also be applied to find solitary frequencies in complex networks by solving equation (21).

ORCID iDs

Jakob Niehues  <https://orcid.org/0000-0003-0140-6910>

Serhiy Yanchuk  <https://orcid.org/0000-0003-1628-9569>

Rico Berner  <https://orcid.org/0000-0003-4821-3366>

Jürgen Kurths  <https://orcid.org/0000-0002-5926-4276>

Frank Hellmann  <https://orcid.org/0000-0001-5635-4949>

References

- [1] Pikovsky A, Rosenblum M and Kurths J 2001 *Synchronization: A universal Concept in Nonlinear Sciences*, (Cambridge Nonlinear Science Series) (Cambridge University Press)
- [2] Strogatz S H 2000 *Physica D* **143** 1
- [3] Acebrón J A, Bonilla L L and Spigler R 2000 *Phys. Rev. E* **62** 3437
- [4] Acebrón J A, Bonilla L L, Pérez Vicente C J, Ritort F and Spigler R 2005 *Rev. Mod. Phys.* **77** 137
- [5] Pecora L M, Sorrentino F, Hagerstrom A M, Murphy T E and Roy R 2014 *Nat. Commun.* **5** 4079
- [6] Rodrigues F A, Peron T K D M, Ji P and Kurths J 2016 *Phys. Rep.* **610** 1
- [7] Kuramoto Y 1984 *Chemical oscillations, waves and turbulence Springer Series in Synergetics* 1st edn (Springer)
- [8] Munyayev V O, Bolotov M I, Smirnov L A, Osipov G V and Belykh I 2023 *Phys. Rev. Lett.* **130** 107201
- [9] Kovalenko K, Dai X, Alfaro-Bittner K, Raigorodskii A M, Perc M and Boccaletti S 2021 *Phys. Rev. Lett.* **127** 258301
- [10] Tanaka H-A, Lichtenberg A J and Oishi S 1997 *Phys. Rev. Lett.* **78** 2104
- [11] Tanaka H-A, Lichtenberg A J and Oishi S 1997 *Physica D* **100** 279
- [12] Bergen A and Hill D 1981 *IEEE Trans. Power Appar. Syst.* **PAS-100** 25
- [13] Witthaut D, Hellmann F, Kurths J, Kettmann S, Meyer-Ortmanns H and Timme M 2022 *Rev. Mod. Phys.* **94** 015005
- [14] Ermentrout B 1991 *J. Math. Biol.* **29** 571
- [15] Omelchenko I, Maistrenko Y, Hövel P and Schöll E 2011 *Phys. Rev. Lett.* **106** 234102
- [16] Gelbrecht M, Kurths J and Hellmann F 2020 *New J. Phys.* **22** 033032
- [17] Halekotte L, Vanselow A and Feudel U 2021 *J. Phys. Complex.* **2** 035015
- [18] Berner R, Yanchuk S and Schöll E 2021 *Phys. Rev. E* **103** 042315
- [19] Olmi S, Navas A, Boccaletti S and Torcini A 2014 *Phys. Rev. E* **90** 042905
- [20] Maistrenko Y, Penkovsky B and Rosenblum M 2014 *Phys. Rev. E* **89** 060901
- [21] Jaros P, Maistrenko Y and Kapitaniak T 2015 *Phys. Rev. E* **91** 022907
- [22] Menck P J, Heitzig J, Kurths J and Schellnhuber H 2014 *Nat. Commun.* **5** 3969
- [23] Hellmann F, Schultz P, Jaros P, Levchenko R, Kapitaniak T, Kurths J and Maistrenko Y 2020 *Nat. Commun.* **11** 592
- [24] Jaros P, Brezetsky S, Levchenko R, Dudkowski D, Kapitaniak T and Maistrenko Y 2018 *Chaos* **28** 011103
- [25] Nitzbon J, Schultz P, Heitzig J, Kurths J and Hellmann F 2017 *New J. Phys.* **19** 033029
- [26] UCTE 2006 Final report system disturbance on 4 November 2006 (available at <https://eepublicdownloads.entsoe.eu/clean-documents/pre2015/publications/ce/otherreports/Final-Report-20070130.pdf>) (Accessed 19 December 2022)
- [27] Rohden M, Sorge A, Timme M and Witthaut D 2012 *Phys. Rev. Lett.* **109** 064101
- [28] Zhang X, Hallerberg S, Matthiae M, Witthaut D and Timme M 2019 *Sci. Adv.* **5** eaav1027
- [29] Menck P-J 2014 How wires shape volumes *PhD Thesis* (Humboldt-Universität zu Berlin, Mathematisch-Naturwissenschaftliche Fakultät I)

- [30] Guckenheimer J and Holmes P 2002 Nonlinear oscillations, dynamical systems and bifurcations of vector fields *Applied Mathematical Sciences* 1st edn (Springer)
- [31] Gao J and Efstathiou K 2018 *Phys. Rev. E* **98** 042201
- [32] Yue W, Smith L D and Gottwald G A 2020 *Phys. Rev. E* **101** 062213
- [33] Munyayev V O, Bolotov M I, Smirnov L A, Osipov G V and Belykh I V 2022 *Phys. Rev. E* **105** 024203
- [34] See Supplemental Material at <https://doi.org/10.1088/1367-2630/ad8b63> for animations of the dynamics of an exemplary complex network; an in-depth, self-contained step-by-step derivation of our main results; more numerical studies; an outline of several possible generalizations; more examples and their comparison; and details of the networks used and numerical experiments.
- [35] Halekotte L and Feudel U 2020 *Sci. Rep.* **10** 11783
- [36] Manik D, Witthaut D, Schäfer B, Matthiae M, Sorge A, Rohden M, Katifori E and Timme M 2014 *Eur. Phys. J. Spec. Top.* **223** 2527
- [37] Schultz P, Heitzig J and Kurths J 2014 *Eur. Phys. J. Spec. Top.* **223** 2593–610
- [38] Niehues J 2023 Revelations.jl (<https://doi.org/10.5281/zenodo.12636090>)
- [39] Hata S and Nakao H 2017 *Sci. Rep.* **7** 1121
- [40] Plietzsch A, Kogler R, Auer S, Merino J, Gil-de Muro A, Liße J, Vogel C and Hellmann F 2022 *SoftwareX* **17** 100861
- [41] Motter A E, Myers S A, Anghel M and Nishikawa T 2013 *Nat. Phys.* **9** 191
- [42] Wassmer J, Witthaut D and Kaiser F 2021 *J. Phys. Complex.* **2** 035003
- [43] Menara T, Baggio G, Bassett D and Pasqualetti F 2022 *Nat. Commun.* **13** 4721
- [44] Witthaut D and Timme M 2012 *New J. Phys.* **14** 083036
- [45] Schultz P, Peron T, Eroglu D, Stemler T, Ramírez Ávila G M, Rodrigues F A and Kurths J 2016 *Phys. Rev. E* **93** 062211
- [46] Kaiser F, Latora V and Witthaut D 2021 *Nat. Commun.* **12** 3143
- [47] Taher H, Olmi S and Schöll E 2019 *Phys. Rev. E* **100** 062306
- [48] Klinshov V V, Nekorkin V I and Kurths J 2015 *New J. Phys.* **18** 013004
- [49] Kogler R, Plietzsch A, Schultz P and Hellmann F 2022 *PRX Energy* **1** 013008